ROCKY MOUNTAIN
JOURNAL OF MATHEMATICS
Volume 21, Number 2, Spring 1991

A MATHEMATICAL PROBLEM IN GEOCHEMISTRY: THE REACTION-INFILTRATION INSTABILITY

J. CHADAM* AND P. ORTOLEVA

1. Introduction. When reactive waters flow through a porous medium they can dissolve the minerals and cause changes in porosity. This, through Darcy's law, can alter the flow, giving rise to a feedback mechanism which can cause instabilities in the shape of the porosity level surfaces. This mechanism most certainly is important in many geochemical situations (e.g., the diagenesis and evolution of mineral, oil and gas reservoirs, the dynamics of nuclear and chemical waste repositories, in situ coal gasification, enhanced oil recovery, etc.). Our own interest in the subject arose from trying to understand the occurrence of so-called roll-front redox mineral deposits [**1,3,4**]. No doubt the coupling of this reaction-infiltration instability to the more widely studied multi-phase flow instabilities should lead to a very rich area for further research.

Typically, the essential geochemical processes of relevance to each of the above situations can be modelled mathematically as a system of coupled, highly nonlinear reaction-transport equations [**3,4**]. In general, however, even the simplified versions of these equations arising from overly simplified physical models are too complicated to be studied abstractly or analytically [**5**]. Our approach here (Section 2) is to restrict attention to a physically important class of problems for which the effective reaction zone (where the serious complications appear) is much smaller and less interesting than the scale of the phenomenon being studied. The resulting set of reaction-transport equations can then be studied using matched asymptotics [**5**] to obtain a more amenable moving free boundary problem for the reaction interface [**4,5**] (Section 3). This will allow us to give [**1,5,6**] (Section 4) a mathematical treatment of the evolution of the shape of the reaction interface in terms

* Lecturer and preparer of this report. Others who contributed to various parts of the work described here are: G. Auchmuty, J. Hettmer, D. Hoff, E. Merino, C. Moore, E. Ripley and A. Sen.

Parts of this work were supported by the DOE (USA) and NSERC (Canada).
Received by the editors on December 10, 1987, and in revised form on March 30, 1988.

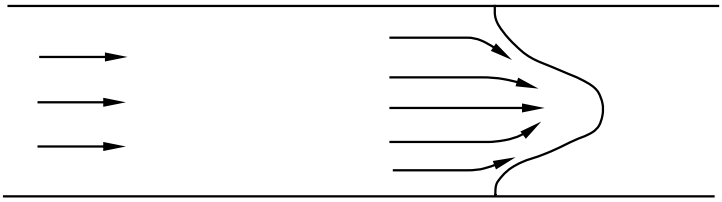

FIGURE 1. Focusing of flow to tip of porosity level curve.

of bifurcation and stability theory. We shall also present (Section 5) the results of some preliminary numerical studies.

2. A Simple reaction-infiltration model. Consider an aquifer consisting of an insoluble porous matrix (e.g., quartz sandstone) with some soluble mineral (e.g., calcite) partially filling the pores. If water is forced through this porous medium, the soluble component will be dissolved out upstream and the water will become saturated sufficiently far downstream.

Between these extremes there is a dissolution zone across which the soluble mineral content—and hence the porosity—changes from its original downstream value to the final, altered value upstream. The question of interest is whether the shape of this dissolution zone is stable. Notice that if a bump (in the porosity level curves) in the reaction zone exists at some time, the flow of the undersaturated waters tends to be focused to the tip of the bump via Darcy's law since inside the bump (on the upstream side) the permeability is greater than in the neighboring regions (see Figure 1). Thus, dissolution is enhanced at the tip causing it to advance more rapidly. This is the porosity change/flow destabilization mechanism. On the other hand, diffusion from the sides of the tip raises the concentration of the solute in the water which is focusing at the tip and hence will decelerate this advancement. The competition between these two processes can lead to decay of the bump, restabilization to a morphologically more complicated dissolution zone or possibly to complete destabilization.

3. Two mathematical models. In this section we write down without details (cf. [**1,5**] for derivations) the models we shall subsequently treat analytically and numerically.

3.1 *Coupled ODE/PDE model.* The rate of increase of the porosity ϕ (equivalently the rate of dissolution of the soluble mineral) is proportional to the reaction rate:

$$\varepsilon \frac{\partial \phi}{\partial t} = -(\phi_f - \phi)^{2/3}(\gamma - 1)(= -R(\phi, \gamma)). \tag{3.1}$$

Here ϕ_f is the final porosity after complete dissolution, γ is the scaled concentration of solute in water (with equilibrium concentration being 1) and $\varepsilon = c_{\text{eq}}/\rho << 1$ is the ratio of the original equilibrium concentration to the density of the soluble mineral. The 2/3-power indicates that we are considering surface reactions. The solute concentration per rock volume, $\phi\gamma$, satisfies a mass conservation equation:

$$\varepsilon \frac{\partial(\phi\gamma)}{\partial t} = \nabla \cdot [\phi D(\phi)\nabla\gamma + \phi\lambda(\phi)\gamma\nabla p] + \frac{\partial \phi}{\partial t} \tag{3.2}$$

where $D(\phi), \lambda(\phi)$ are the porosity dependent, scaled diffusion coefficient and permeability, respectively, and p is the pressure. Darcy's law has been used in the convective term of (3.2). It is also used in combination with the continuity equation to give:

$$\nabla \cdot [\phi\lambda(\phi)\nabla p] = \varepsilon \frac{\partial \phi}{\partial t}. \tag{3.3}$$

In addition, we impose the asymptotic conditions:

$$\gamma \to 0, \qquad \phi \to \phi_f \quad \text{and} \quad \frac{\partial p}{\partial x} \to \frac{\kappa_f p_f'}{D_f} = -\frac{v_f}{D_f} \quad \text{as } x \to -\infty \tag{3.4}$$

and

$$\gamma \to 1, \qquad \phi \to \phi_0, \qquad \frac{\partial p}{\partial x} \to ? \quad \text{as } x \to +\infty. \tag{3.5}$$

These indicate that far upstream the water is fresh ($\gamma = 0$) and the mineral has been completely dissolved out ($\phi = \phi_f$). Also, the pressure

gradient (equivalently the velocity through Darcy's law $v_f = -\kappa_f p_f'$) is specified as in (3.4) with the effects of the scaling appearing explicitly. Far downstream the water is saturated ($\gamma = 1$), the porosity is still at its original, unaltered value ($\phi = \phi_0$) and the pressure gradient (equivalently the velocity) is to be determined. Equations (3.1–5), along with given initial data and zero flux boundary conditions on the transverse boundaries, form a complete problem for the unknowns γ, ϕ, p. Unfortunately, nothing can be calculated analytically from these equations except the velocity of a traveling planar dissolution zone. On the other hand, they form the basis of our numerical simulations which will be discussed later.

3.2 *Moving free boundary model.* In order to obtain an analytically tractable problem, we take the large solid density limit $\varepsilon = c_{\text{eq}}/\rho \to 0$. The dissolution zone, typically of width $\varepsilon^{1/2}$, collapses to a dissolution interface located at $x = R(y,t)$, with R *unknown*. Then, off this interface there is no reaction and the only consistent way to satisfy equations (3.1–3) to all orders of ε is as follows. Upstream of the dissolution interface where from scaling $\lambda(\phi_f)$ and $D(\phi_f) = 1$, one has

$$\left.\begin{aligned} &\Delta\gamma + \nabla\gamma \cdot \nabla p = 0 && (3.6)\\ &\phi = \phi_f && (3.7)\\ &\Delta p = 0 && (3.8) \end{aligned}\right\} \quad \text{in } x < R(y,t), \quad 0 \le y \le L$$

while downstream one obtains

$$\left.\begin{aligned} &\gamma \equiv 1 && (3.9)\\ &\phi = \phi_0 && (3.10)\\ &\Delta p = 0 && (3.11) \end{aligned}\right\} \quad \text{in } x > R(y,t), \quad 0 \le y \le L$$

where we have taken $\phi_0(x,y,0) = \phi_0$, constant, to show that the morphological instabilities will even occur in this spatially homogeneous situation. Besides the asymptotic conditions (3.4, 5), one also obtains, via matched asymptotics, boundary conditions on the unknown moving dissolution interface. Specifically, we shall study variations normal to the interface on a scale of $O(\varepsilon^{1/2})$. If σ is the coordinate normal to the interface, then (3.3) becomes

$$\nabla \cdot (\phi\lambda(\phi)\nabla p) = \varepsilon \left(\frac{\partial \phi}{\partial t} - \mu \frac{\partial \phi}{\partial \sigma} \right) \tag{3.12}$$

where μ is the normal velocity of the front. Expanding all quantities in powers of $\varepsilon^{1/2}$ we have

$$p = p_0 + \varepsilon^{1/2} p_1 + \dots, \tag{3.13a}$$

$$\phi = \phi_0 + \varepsilon^{1/2} \phi_1 + \dots, \tag{3.13b}$$

$$\gamma = \gamma_0 + \varepsilon^{1/2} \gamma_1 + \dots, \tag{3.13c}$$

$$\mu = \mu_0 + \varepsilon^{1/2} \mu_1 + \dots . \tag{3.13d}$$

For the "inner" behavior within the interface (i.e., for small σ) we consider the above to be functions of a stretched variable $\xi = \varepsilon^{-1/2}\sigma$ and the tangent variables $\underline{r}_T$. Inserting these into (3.12) and collecting terms to various orders in $\varepsilon^{1/2}$, we find, to leading order, ε^{-1}, the equation

$$\frac{\partial}{\partial \xi}\left(\phi_0 \lambda(\phi_0) \frac{\partial p_0}{\partial \xi}\right) = 0. \tag{3.14}$$

This shows that $\phi_0 \lambda(\phi_0) \partial p_0 / \partial \xi$ is a constant throughout the interfacial region. But away from the interface ($|\xi| \to \infty$), the pressure is a smooth function (satisfying $\Delta p = 0$) and hence $\partial p / \partial \xi \to 0$ as $|\xi| \to \infty$. Thus the value of this constant must be zero. Since ϕ_0 and $\lambda(\phi_0)$ do not vanish at the interface, it follows then that $\partial p_0 / \partial \xi = 0$ or p_0 remains continuous across the interface.

At the next order, $\varepsilon^{-1/2}$, we find

$$\frac{\partial}{\partial \xi}\left(\phi_0 \lambda(\phi_0) \frac{\partial p_1}{\partial \xi}\right) = 0. \tag{3.15}$$

Matching the outer limit of the derivative of the inner solution ($|\xi| \to \infty$) with the inner limit of the derivative of the outer solution ($S \to 0\pm$) we have

$$\lim_{\xi \to \pm\infty} \frac{\partial p_1}{\partial \xi} = \lim_{S \to 0\pm} \frac{\nabla S}{|\nabla S|} \cdot \nabla p_0 = \lim_{S \to 0\pm} \frac{\partial p_0}{\partial n}. \tag{3.16}$$

Combining (3.16) with the integral from $\xi = -\infty$ to $\xi = +\infty$ of (3.15) one finds the jump condition in the pressure gradient across the interface to be given by

$$\lim_{S\to 0-} \frac{\partial p_0}{\partial n} = \left(\lim_{S\to 0-} \phi_0 \lambda(\phi_0) / \lim_{S\to 0+} \phi_0 \lambda(\phi_0) \right) \lim_{S\to 0+} \frac{\partial p_0}{\partial n}. \tag{3.17}$$

In the notation of (3.6–3.11) these jump conditions at the interface can be written as

$$p- = p+, \tag{3.18}$$

$$\frac{\partial p-}{\partial x} - \frac{\partial p-}{\partial y} \cdot \frac{\partial R}{\partial y} = \Gamma \left(\frac{\partial p+}{\partial x} - \frac{\partial p+}{\partial y} + \frac{\partial R}{\partial y} \right), \quad \left.\begin{array}{c} \text{on} \\ X = R(y,t) \\ 0 \le y \le L, \end{array}\right\} \tag{3.19}$$

where $0 \le r = \phi_0 \lambda_0 / \phi_f \lambda_f = \phi_0 \kappa_0 / \phi_f \kappa_f$ is a measure of the porosity change. A similar matching analysis on equation (3.2) gives the jump conditions

$$\gamma \equiv 1 \tag{3.20}$$

$$\frac{\partial \gamma}{\partial x} - \frac{\partial \gamma}{\partial y} \cdot \frac{\partial R}{\partial y} = (1 - \phi_0/\phi_f) R_t, \quad \left.\begin{array}{c} \text{on} \\ X = R(y,t) \\ 0 \le y \le L. \end{array}\right\} \tag{3.21}$$

Equation (3.21) relates the rate of advancement of the moving dissolution interface to the flux of the concentration and is called a Stefan condition. A final scaling $x' = (\pi/L)x$, $y' = (\pi/L)y$, $t' = (\pi/L)^2(1 - \phi_0/\phi_f)^{-1} t$ with $R' = (\pi/L)R$ (and dropping the primes) makes the transverse dimension $0 \le y \le \pi$, and results in the two changes

$$\gamma \to 0, \qquad \phi \to \phi_f, \qquad \frac{\partial p}{\partial x} \to -\frac{v_f L}{D_f \pi} \quad \text{as } x \to -\infty \tag{3.4'}$$

and

$$\frac{\partial \gamma}{\partial x} - \frac{\partial \gamma}{\partial y} \cdot \frac{\partial R}{\partial y} = R_t \quad \text{on} \quad x = R(y,t), 0 \le y \le \pi. \tag{3.21'}$$

Problem $(3.4', 5, \ldots 11, 18 \ldots 21')$ with initial conditions and zero flux transverse conditions on $y = 0$, π is the version we shall examine analytically in the next section. Notice that only two essential parameters

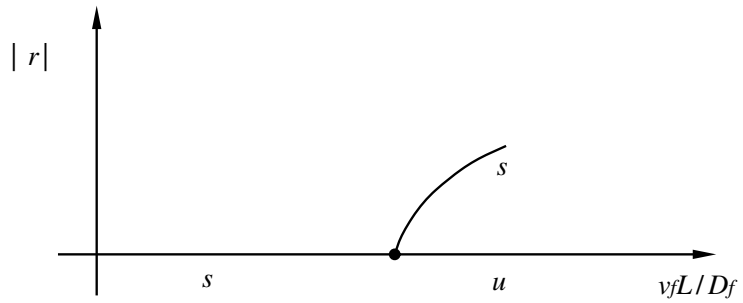

FIGURE 2. Pitchfork stability diagram indicating loss of stability of planar ($\delta r = 0$) to nonplanar ($\delta r \neq 0$) solutions in terms of the bifurcation parameter $v_f L/D_f$.

remain in the problem, the dynamical parameter $\nu_f = v_f L/D_f$ and the measure of the porosity change $\Gamma = \phi_0\kappa_0/\phi_f\kappa_f$.

4. Shape instabilities. In this section we describe our analytical results [**5,6**] in the context of the large solid density problem $(3.4', 5, 11, 18, 21')$. This free boundary problem is different from but not unrelated to those which arise by similar limiting procedures in combustion [**7**], solidification [**2**], electrochemical forming and machining [**8**], etc., and is tractable by similar techniques. Here the planar, constant velocity solution can be obtained explicitly and completely, including the concentration and pressure profiles which were not available for the more general coupled ODE/PDE model. The linearized stability of this solution is then described, giving a precise value of the parameter ν_f (in terms of Γ) for which the planar solution loses stability to another, more structured, solution. In the language of bifurcation theory we determine the critical parameter value for which the spectrum of the linearized problem changes sign from negative to positive, thus determining the location of a possible bifurcation point. Finally we sketch the local bifurcation analysis to show that the linear instabilities are restabilized by the nonlinearities to a morphologically more complicated solution. More specifically, we shall obtain a Landau equation for the amplitude of the linearly unstable mode, thus indicating a standard pitchfork bifurcation diagram as in Figure 2.

4.1 *Planar solution.* Denoting the planar state quantities with a super bar, one can easily check [**5,6**] that the following constant velocity solution satisfies problem $(3.4', 5, \ldots 11, 18, 21')$:

$$\overline{R}(t) = \overline{V}t \tag{4.1}$$

$$\overline{\gamma}(x,t) = \begin{cases} e^{-\overline{\nu}_f(x-\overline{V}t)} & x < \overline{V}t \\ 1 & x > \overline{V}t \end{cases} \tag{4.2}$$

$$\overline{p}(x,t) = \begin{cases} -\overline{\nu}_f(x-\overline{V}t) & x < \overline{V}t \\ -\overline{\nu}_0(x-\overline{V}t) & x > \overline{V}t \end{cases} \tag{4.3}$$

where $\overline{\nu}_f = \nu_f/\pi = V_f L/D_f\pi$, $\overline{\nu}_0 = \phi_f\overline{\nu}_f$ (from (3.5) and (3.19)) and the velocity of the planar interface $\overline{V} = \overline{\nu}_f$ from $(3.21')$.

4.2 *Linear shape instability.* In order to examine the stability of the above planar solutions (4.1,3) with respect to bumps we consider perturbations of the type (i.e., a generic term in the Fourier decomposition—only cosine terms appear because of the zero flux transverse boundary conditions)

$$R(y,t) = \overline{V}t + \delta r_{\rm m}(t)\cos my \tag{4.4a}$$

$$\gamma(x,y,t) = \overline{\gamma}(x,t) + \delta\gamma_{\rm m}(x)r_{\rm m}(t)\cos my \tag{4.4b}$$

$$p(x,y,t) = \overline{p}(x,t) + \delta p_{\rm m}(x)r_{\rm m}(t)\cos my. \tag{4.4c}$$

Considering δ to be small, the linearized version of equations $(3.4', 5, \ldots 11, 18, \ldots 21')$ can be derived [**5**] (i.e., retain terms in first power of δ). These can be solved explicitly for $\gamma_{\rm m}$ and $p_{\rm m}$ and the Stefan condition gives [**5,6**] the following condition on the amplitude $r_{\rm m}(t)$ of the $\cos my$ bump:

$$r'_{\rm m}(t) = \frac{\overline{\nu}_f}{1+\Gamma}\left(\overline{\nu}_f - (\overline{\nu}_f^2 + 4m^2)^{1/2} + (1-\Gamma)|m|\right) r_{\rm m}(t). \tag{4.5a}$$

This differential equation indicates that the amplitude of the bump grows or decays depending on the sign of the coefficient. The connection with the equivalent, more conventional viewpoint follows by expressing

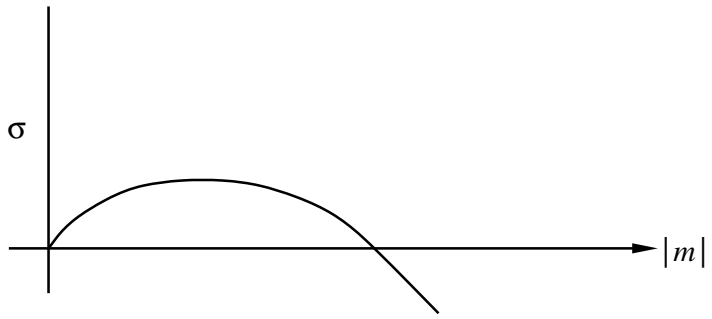

FIGURE 3. Graph of dispersion relation (4.5b).

$r_{\mathrm{m}}(t) = re^{\sigma(m)t}$ in terms of the spectrum $\sigma(m)$ of the linearized problem and obtaining from (4.5a) the dispersion relation

$$\sigma(m) = \frac{\overline{\nu}_f}{1+\Gamma}\left(\overline{\nu}_f - (\overline{\nu}_f^2 + 4m^2)^{1/2} + (1-\Gamma)|m|\right). \tag{4.5b}$$

The m-dependence of σ is shown in Figure 3 revealing clearly that the planar solution (4.1,3) is linearly unstable to long wavelength perturbations (because $\Gamma < 1$) and stable to short wavelength perturbations. The critical wave number ($|m_0|$ at which $\sigma(m_0) = 0$) is given by

$$|m_0| = \frac{2(1-\Gamma)}{(3-\Gamma)(1+\Gamma)}\overline{\nu}_f. \tag{4.6}$$

Since our channel width has been normalized to π, the first mode which can be carried is $|m_0| = 1$ giving, from (4.6), the critical parameter value (of $\nu_f = v_f L/D_f$)

$$\nu_c = \nu_c(\Gamma) = \frac{(3-\Gamma)(1+\Gamma)\pi}{2(1-\Gamma)}. \tag{4.7}$$

From this we see that the instability does indeed arise analytically and that, as is physically realistic, larger flow speeds, larger transverse dimensions, larger porosity/permeability changes promote the instability while larger diffusion coefficients inhibit the instability (i.e., diffusion is stabilizing, as mentioned earlier). The limit of $\Gamma \to 1$ (i.e., no porosity

change) suggests it is very difficult to produce instabilities. This has been verified by a separate analysis [**1**]. Thus, this instability can occur only if "significant" amounts of the soluble mineral are dissolved.

4.3 *Nonlinear restabilization.* We begin by scaling the independent variables. Because the instability occurs at finite wavelength none is required for the spatial variables while, as is common for a (anticipated) pitchfork bifurcation,

$$t_2 = \varepsilon^2 t. \tag{4.8}$$

Additionally, we write

$$\nu_f = \nu_c + \varepsilon\nu_1 + \varepsilon^2\nu_2 + \cdots . \tag{4.9}$$

We find [**6**] at $O(\varepsilon^2)$ that $\nu_1 = 0$ (as usual for pitchfork bifurcations) so that the physical significance of the small parameter ε is

$$\varepsilon \simeq (\nu_f - \nu_c)^{1/2} \tag{4.10}$$

where we have taken, without loss of generality, $\nu_2 = 1$. Thus,

$$\nu_f = \nu_c + \varepsilon^2 + \varepsilon^3\nu_3 + \cdots . \tag{4.11}$$

The stability calculation then proceeds by expanding all of the dependent variables in terms of ε (suppressing the sub-2 in the new t_2 variable):

$$\begin{aligned} R(y,t) = {} & \overline{V}(\varepsilon)t \\ & + \varepsilon(r_{10}(t) + r_{11}(t)\cos y + r_{12}(t)\cos 2y + \cdots) \\ & + \varepsilon^2(r_{20}(t) + r_{21}\cos y + r_{22}(t)\cos 2y + \cdots) \\ & + \varepsilon^3(r_{30}(t) + r_{31}\cos y + r_{23}(t)\cos 2y + \cdots) \\ & + O(\varepsilon^4), \end{aligned} \tag{4.12a}$$

$$\begin{aligned} \gamma(x,y,t) = {} & \overline{\gamma}(x,t;\varepsilon) \\ & + \varepsilon(\gamma_{10}(x,t) + \gamma_{11}(x,t)\cos y + \gamma_{12}(x,t)\cos 2y + \cdots) \\ & + \varepsilon^2(\gamma_{20}(x,t) + \gamma_{21}(x,t)\cos y + \gamma_{22}(x,t)\cos 2y + \cdots) \\ & + \varepsilon^3(\gamma_{30}(x,t) + \gamma_{31}(x,t)\cos y + \gamma_{32}(x,t)\cos 2y + \cdots) \\ & + O(\varepsilon^4), \end{aligned} \tag{4.12b}$$

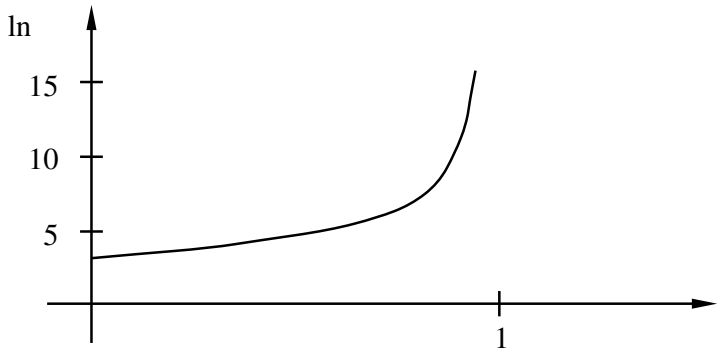

FIGURE 4. Graph of the logarithm of the Landau constant versus $\Gamma = \phi_0\kappa_0/\phi_f\kappa_f$, a measure of the porosity change.

and similarly for $p(x, y, t)$. Following the prescription outlined in standard weakly nonlinear stability analysis (except that the equations are solved directly rather than obtaining conditions from the orthogonality of inhomogeneous terms and solutions of the homogeneous problem) one obtains a Landau differential equation for the amplitude of the unstable mode, $r_{11}(t)$:

$$r'_{11}(t) = wr_{11}(t) - \Lambda r_{11}(t)^3 \tag{4.13}$$

where

$$w = w(\Gamma) = \frac{\nu_c}{1+\Gamma}\,\frac{((\nu_c^2+4)^{1/2} - \nu_c)}{(\nu_c^2+4)^{1/2}} \geq 0 \tag{4.14}$$

and the Landau constant, $\Lambda = \Lambda(\Gamma)$, which is algebraically very complicated, is given in Figure 4. The positivity of Λ indicates that in the vicinity of the critical point the linearized instabilities (from $w \geq 0$) are restabilized by the nonlinearities at the next highest order and from (4.13) that the bifurcation diagram is the symmetric pitchfork. The asymptotic amplitude of the bump can be obtained from (3.13) to be $(w/\Lambda)^{1/2}$.

5. Numerical simulations. The actual shape of the stabilized bump, especially far from the critical point (to which the analysis

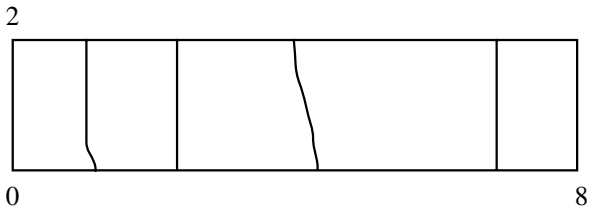

FIGURE 5A. $\nu_f << \nu_c$. Evolution of porosity level curve for times $0.0, 1.8, 3.6, 5.4$.

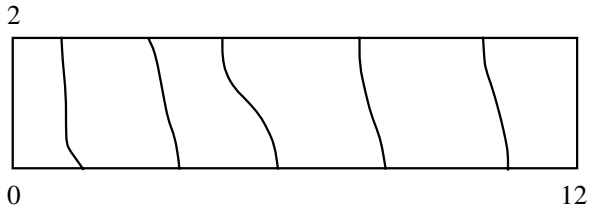

FIGURE 5B. $\nu_f \simeq \nu_c$. Evolution of porosity level curve for times $0.0, 1.5, 3.0, 3.75$.

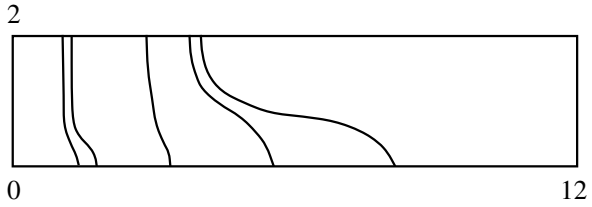

FIGURE 5C. $\nu_f >> \nu_c$. Evolution of porosity level curves for times $0.0, .24, .48, .72, .96$.

of the last section does not apply) must be obtained from numerical simulations. Because interface tracking is a difficult problem we return to the coupled ODE/PDE model with $\varepsilon = c_{\text{eq}}/\rho$ small ($= 0.05$) but not zero. Using parameter values suggested by the analytical results of the previous section and standard numerical methods [**5**] for solving equations (3.1–5), we investigated the three cases $\nu_f << \nu_c$, $\nu_f \simeq \nu_c$ and $\nu_f >> \nu_c$. Figures 5a, b, c depict these cases, respectively, indicating stability of the planar front, restabilization to a new shape and a highly unstable dissolution zone, respectively.

REFERENCES

1. J. Chadam, G. Auchmuty, E. Merino, P. Ortoleva and E. Ripley, *The structure and stability of moving redox fronts*, SIAM J. Appl. Math. **46** (1986), 588–604.

2. ——— and P. Ortoleva, *The stabilizing effect of surface tension on the development of the free boundary in a planar one-dimensional Cauchy-Stefan problem*, IMA J. Appl. Math. **30** (1983), 57–66.

3. ———, ———, E. Merino and C. Moore, *Geochemical self-organization I: Feedback mechanisms and modeling approach*, Amer. J. Sci. **287** (1987), 979–1007.

4. ———, ———, ——— and A. Sen, *Self-organization in water-rock interaction systems, II: The reactive-infiltrate instability*, Amer. J. Sci. **287** (1987), 1008 –1040.

5. ———, ——— and A. Sen, *Reactive infiltration instabilities*, IMA J. Appl. Math **36** (1986), 207–220.

6. ———, ——— and ———, *Weakly nonlinear stability of reaction-percolation interfaces*, SIAM J. Appl. Math. **48** (1987), 1362–1378.

7. B.J. Matkowsky and G.I. Shivashinsky, *Propagation of a pulsating reaction front in solid fuel combustion*, SIAM J. Appl. Math. **35** (1978), 465–478.

8. J.A. McGeough, *Principles of electrochemical machining*, Chapman and Hall, London, 1974.

Department of Mathematics and Statistics, McMaster University, Hamilton, Ontario, Canada L8S 4K1

Departments of Chemistry & Geology, Indiana University, Bloomington, Indiana, USA 47405